

THE CALIPSO MISSION

A Global 3D View of Aerosols and Clouds

BY D. M. WINKER, J. PELON, J. A. COAKLEY JR., S. A. ACKERMAN, R. J. CHARLSON, P. R. COLARCO, P. FLAMANT, Q. FU, R. M. HOFF, C. KITAKA,* T. L. KUBAR, H. LE TREUT, M. P. MCCORMICK, G. MÉGIE,* L. POOLE, K. POWELL, C. TREPTE, M. A. VAUGHAN, AND B. A. WIELICKI

CALIPSO, with CloudSat, provides the first multiyear global view of the vertical structure of aerosols and clouds, which is crucial to determining their role in the climate system

The energy that drives Earth's climate system comes from the sunlight absorbed by the Earth. For a climate in equilibrium, there is an energy balance between this absorbed sunlight and thermal radiation to space (Trenberth et al. 2009). Aerosols and clouds affect Earth's energy budget by reflecting sunlight back to space, which cools the Earth, and by absorbing sunlight and trapping outgoing thermal radiation, which warms the Earth. Anthropogenic aerosols are known to significantly affect the net global radiation budget (Charlson et al. 1992) but quantifying the effects has proven difficult. The numerous influences of clouds on Earth's energy budget have long been the subject of study (Hartmann et al. 1992), but the need to provide measurements capable of constraining climate feedbacks places stringent requirements on observing systems (Zhang et al. 2004). The sensitivity of the climate to forcings by aerosols, greenhouse gases, and other sources is largely controlled by interactions among clouds, radiation, and

atmospheric circulation (Randall et al. 1989; Wielicki et al. 1995). The need to predict these interactions has challenged both our abilities to observe aerosols and clouds globally and to represent them in global climate models.

Because both water droplets and ice crystals typically nucleate on small aerosol particles, changes in the concentration or properties of these aerosols can influence cloud formation and cloud radiative properties. Aerosols may either suppress or enhance precipitation, thus affecting the water cycle and latent as well as radiative heating. The cloud environment may also alter aerosol properties through hygroscopic growth in the humid air between clouds or through in-cloud processing of the aerosol. Clouds act to distribute aerosols by transporting particles and particle precursors from the boundary layer to the free troposphere. Clouds also remove particles and their precursors from the lower atmosphere through in-cloud chemistry and precipitation. Thus, many

AFFILIATIONS: WINKER, POWELL, TREPTE, VAUGHAN, AND WIELICKI—NASA Langley Research Center, Hampton, Virginia; PELON AND MÉGIE—Université Pierre et Marie Curie, CNRS-INSU, IPSL, LATMOS, Paris, France; COAKLEY—College of Oceanic and Atmospheric Sciences, Oregon State University, Corvallis, Oregon; ACKERMAN—Cooperative Institute for Meteorological Satellite Studies, University of Wisconsin—Madison, Madison, Wisconsin; CHARLSON AND FU—Department of Atmospheric Sciences, University of Washington, Seattle, Washington; COLARCO—NASA Goddard Space Flight Center, Greenbelt, Maryland; FLAMANT—École Polytechnique, LMD, IPSL, Palaiseau, France; HOFF—University of Maryland, Baltimore County, Baltimore, Maryland; KITAKA AND POOLE—Science Systems and Applications, Inc., Hampton, Virginia; KUBAR—Jet Propulsion Laboratory, California Institute of

Technology, Pasadena, California; LE TREUT—Université Pierre et Marie Curie, ENS, École Polytechnique, CNRS-INSU, IPSL, LMD, Paris, France; MCCORMICK—Hampton University, Hampton, Virginia
*Deceased

CORRESPONDING AUTHOR: David Winker, NASA Langley Research Center, Hampton, VA 23681-2199
E-mail: david.m.winker@nasa.gov

The abstract for this article can be found in this issue, following the table of contents.

DOI:10.1175/2010BAMS3009.1

In final form 11 February 2010
©2010 American Meteorological Society

intricate processes link clouds and aerosols with the larger climate system. The roles played by aerosols and clouds in the climate system and how these roles may change in the future are the source of much of the current uncertainty in predicting global change (Solomon et al. 2007).

Over the last several decades, satellite remote sensing has provided an increasingly detailed view of aerosols and clouds (Rossow and Schiffer 1999; King et al. 1999; Kaufman et al. 2002). Yet, until very recently, our ability to study their vertical structure was limited. Launched in April

2006, the CALIPSO mission was conceived and developed to provide new insights into aerosols and clouds, their various interactions, and their roles in the climate system. CALIPSO carries CALIOP (rhymes with “eye-oh-pea”), a nadir-viewing two-wavelength, polarization-sensitive lidar, along with two passive sensors: the WFC and the IIR (Fig. 1). CALIOP is the first polarization lidar in orbit and the first satellite lidar to provide long-term continuous measurements. Combining coincident observations from the lidar and the passive sensors offers new possibilities for retrieving the properties of clouds and aerosols. CALIPSO flies as part of the A-train constellation of satellites (Stephens et al. 2002), offering a variety of additional measurement synergies and now providing the first multiyear dataset of global aerosol and cloud profiles. In this paper we provide an overview of the mission and highlight early results.

SCIENCE CHALLENGES AND MEASUREMENT STRATEGY. *Aerosols: Direct forcing and interactions with clouds.*

The largest uncertainties in climate forcings have been identified as the aerosol direct and indirect radiative forcings (Solomon et al. 2007). Aerosol particles directly affect Earth’s energy budget by scattering and absorbing sunlight and, to a lesser extent, absorbing and emitting infrared radiation. These processes contribute to the aerosol direct radiative forcing. Aerosol layers often include tiny particles known as cloud condensation nuclei, around which water condenses to form cloud drop-

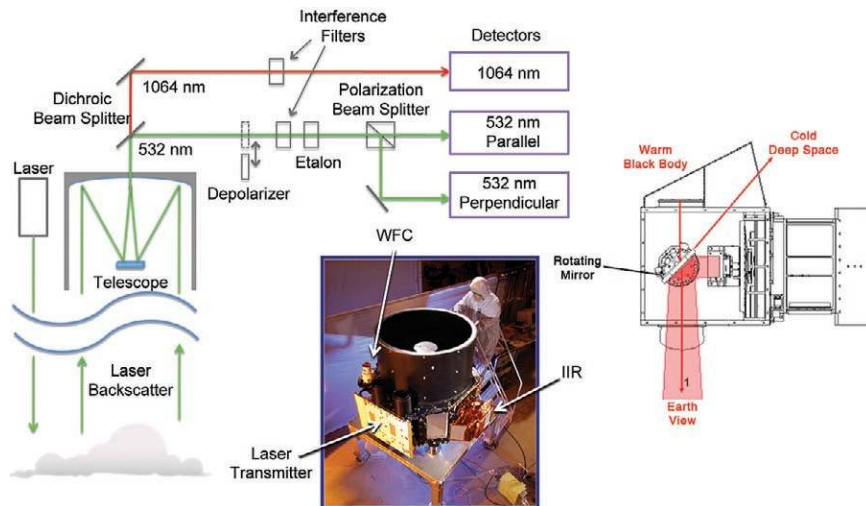


FIG. 1. The CALIPSO payload. CALIOP has a two-wavelength laser transmitter and a three-channel receiver. The IIR is a three-channel infrared radiometer. The WFC is a visible imager with a single channel. The two passive sensors image a 60-km swath centered on the lidar footprint. (Payload photograph courtesy of Ball Aerospace Technology Corporation.)

lets, and ice nuclei around which water freezes to form ice crystals. Aerosols thus affect the sizes and number concentrations of water droplets and ice crystals, which in turn affect the radiative properties of the clouds. These processes, first recognized by Twomey (1977), are referred to as the Twomey effect and contribute to the aerosol indirect radiative forcing. By changing the sizes and concentrations of water droplets and ice crystals, aerosols also affect the ways in which clouds interact with the surrounding atmosphere, giving rise to further changes in their properties, changes in their lifetimes, the concentrations of condensed and frozen water, the formation of precipitation, and the volume of the atmosphere that is cloudy. These additional effects contribute to cloud–climate feedbacks (Lohmann and Feichter 2005; Solomon et al. 2007).

Compared with the effects of greenhouse gases, identifying and quantifying the effects of aerosols on climate is much more difficult. The composition and properties of atmospheric aerosols are highly variable because the aerosols originate from a variety of sources through a number of different mechanisms. With atmospheric lifetimes on the order of a week, they can be transported across continents and oceans, but they do not remain in the atmosphere long enough to become uniformly mixed globally. Consequently, their distribution and properties are highly variable geographically, temporally, and vertically. This variability contributes to the wide range of estimates for the aerosol direct radiative forcing (−0.9

to -0.1 W m^{-2} ; Solomon et al. 2007). Interestingly, estimates based primarily on satellite observations show a negative bias relative to model-based estimates. Passive satellites only retrieve aerosol properties in cloud-free columns. Current satellite aerosol climatologies are restricted to clear-sky conditions, and observation-based estimates of aerosol direct radiative forcing are sensitive to the assumptions invoked to estimate the all-sky forcing (Yu et al. 2006; Bellouin et al. 2008). Resolving the differences among the various estimates requires new datasets representing more than just clear-sky conditions and providing more robust observational tests of models.

Passive satellites measure column-averaged aerosol properties. They have limited capabilities to resolve the vertical distribution of aerosols within the atmosphere, yet the effects of aerosol on climate depend critically on this distribution, especially relative to that of clouds. For example, Quijano et al. (2000) and Penner et al. (2003) show that models must place overlapping aerosol and cloud layers correctly in the vertical to compute accurate radiative fluxes. Chung et al. (2005) show a factor of 6 range in aerosol direct forcing, depending on the relative vertical distributions of overlapping cloud and absorbing aerosol. Furthermore, heating by absorbing aerosols can lead to cloud dissipation when the cloud is embedded in the aerosol layer or the aerosol is located immediately above the layer (Ackerman et al. 2000). On the other hand, if an absorbing aerosol is located well above the cloud layer, it can produce a cooling at cloud level, enhancing cloud formation.

The radiative forcing from the indirect effect of aerosols on clouds is poorly understood (Lohmann and Feichter 2005). There are a number of observational difficulties in determining these effects from satellite observations, but one fundamental problem is the inability of passive satellite sensors to retrieve the vertical profile of aerosols. Column AOD is often used as a proxy for the concentration of aerosols affecting clouds, but the AOD may be poorly correlated with the aerosol concentration at cloud level. The aerosol layer can even be above or beneath the cloud which is presumed to be affected, but separated from the cloud by a layer of clear air. Furthermore, aerosol particles are also affected by the near-cloud thermodynamic environment (Matheson et al. 2005; Twohy et al. 2009; Tackett and Di Girolamo 2009), and the enhancement in the illumination arising from the scattering of sunlight by clouds biases the aerosol properties retrieved in nearby clear-sky columns (Wen et al. 2007; Marshak et al. 2008). Finally, Twomey predicted a negative correlation between aerosol optical depth

and cloud droplet effective radius. Such correlations are often found (Nakajima et al. 2001; Sekiguchi et al. 2003; Matheson et al. 2005; Kaufman et al. 2005; among others), but they can arise in part through an inability to distinguish between “clear” and “cloudy” air (Matheson et al. 2006; Charlson et al. 2007). CALIOP provides new capabilities to distinguish optically thin boundary layer cloud from aerosol by considering the vertical thickness and location of the layers as well as from the spectral behavior of the lidar backscatter. Global observations made with the CALIPSO lidar in conjunction with other A-train instruments will help quantify many of these current uncertainties.

Cloud–climate feedbacks. “Climate sensitivity,” which is the change in global mean surface temperature per unit radiative forcing, is a key parameter characterizing climate change. The climate sensitivity depends on the effects of a variety of feedback processes that may act to amplify or diminish the direct response of the climate to radiative forcings. Cloud feedbacks are the dominant source of the current factor of 3 range in climate model sensitivity (Solomon et al. 2007; Dufresne and Bony 2008). Differences in the cloud parameterizations used in the various models lead to significant differences in the modeled response of clouds to climate change. This situation has changed little over the last two decades (Cess et al. 1990). Reducing current uncertainties in modeled cloud feedback processes requires improved global cloud datasets that are able to resolve the ambiguities of cloud properties in the existing cloud climatologies. Many of these ambiguities arise from the lack of reliable information on the vertical structure of clouds and cloud properties, which CALIPSO and CloudSat can now provide.

First, CALIPSO observations are proving invaluable in testing the adequacy of retrieval schemes used with passive sensors to produce the cloud properties that feed into the climatologies. CALIOP return signals are highly sensitive to the presence of cloud. Cloud altitude is observed directly, and cloudy and cloud-free columns traversed by the lidar beam are clearly distinguished. With passive sensors, the properties of multilayered cloud systems are often interpreted in terms of an “effective” cloud layer at an altitude somewhere between that of the uppermost and lowermost cloud layers. Because the lidar beam often penetrates thin cirrus overlying lower-level cloud layers, CALIOP observations provide new assessments of the occurrence of low-level clouds (see “The occurrence of marine stratus and stratocumulus” for more information).

Second, CALIPSO observations are unique in their ability to identify and characterize thin upper layers of cirrus located above lower-level clouds. Small variations in thin cirrus can have effects on cloud radiative forcing that are comparable in magnitude to the radiative forcing due to human activity. For the same amount of condensed water, ice crystals and supercooled cloud water droplets have very different radiative effects (Sun and Shine 1995). Furthermore, changes in ice crystal shapes, sizes, and orientation can all have significant effects (Yang et al. 2007). Model assumptions controlling the cloud ice/water phase have significant effects on GCM predictions of climate sensitivity (Li and Le Treut 1992; Fowler and Randall 1996). Observations of the distribution of ice and water clouds could provide constraints on modeled cloud feedbacks at middle and high latitudes (Tsushima et al. 2006), but existing satellite datasets are plagued by ambiguities in separating ice, water, and mixed-phased clouds (Platnick et al. 2003; Doutriaux-Boucher and Quaas 2004). The CALIPSO mission, with its combination of polarization lidar and infrared measurements, provides new tools for probing these clouds and assessing their effect on Earth's energy budget.

Measurement strategy. The goal of CALIPSO is to provide a new observational dataset that will lead to improvements in the performance of a variety of atmospheric models ranging from global climate, weather forecast, and air quality models to small-scale cloud-resolving models. From the beginning, the strategy was to acquire coincident measurements from active and passive sensors to take advantage of the strengths of each. Consequently, CALIPSO was initially proposed to fly with the EOS *Aqua* satellite to provide profile information to supplement the observations of aerosol, cloud, and radiative fluxes being acquired by the MODIS, AIRS, and CERES instruments. The proposal led to the current A-train constellation that now includes *Aqua*, *Aura*, CALIPSO, CloudSat, and PARASOL (Stephens et al. 2002). CALIPSO and the other satellites of the A-train fly in a 705-km sun-synchronous polar orbit providing global coverage between 82°N and 82°S. The CALIPSO orbit is controlled to maintain formation with the *Aqua* satellite, and the orbit of CloudSat is controlled to maintain close formation with CALIPSO (now flying about 12 s ahead), ensuring the acquisition of collocated nearly coincident measurements.

THE CALIPSO MISSION. CALIPSO was developed as part of the NASA ESSP program in collabora-

tion with France's CNES with the intention to fill gaps in our ability to observe the global distribution and properties of aerosols and clouds (Winker et al. 2003). CALIPSO was launched together with CloudSat into the A-train orbit in April 2006. While lower orbits are more favorable to active sensors, allowing higher

THE OCCURRENCE OF MARINE STRATUS

Cloud cover over the global oceans is dominated by low-level marine stratocumulus. As these clouds lie just above the underlying surface, their effect on the longwave radiation that Earth emits to space is relatively small, but these clouds reflect considerable sunlight. Such clouds alone contribute nearly 60% of the net cloud radiative forcing in the climate system (Hartmann et al. 1992). They also prove to be major sources of uncertainty in climate sensitivity (Bony and Dufresne 2005). A-train observations, and particularly the CALIPSO–CloudSat observations, are paving the way to gaining improved characterizations of these cloud systems and how they transition from extensive layers of marine stratus and stratocumulus in the subtropical highs along the eastern boundaries of the Atlantic and Pacific in both the Northern and Southern Hemispheres to shallow trade wind cumulus and then deep convection as the equator is approached. Figure SBI.1a shows cloud-top heights obtained from CALIPSO and CloudSat as given in the merged radar–lidar cloud geometrical profile product CloudSat 2B-GEOPROF-lidar, combined with temperature and humidity profiles from collocated ECMWF analyses. The observations cover a transect that extends from the equatorial central Pacific to the west coast of North America. Middle and deep convection are most prevalent between 0° and 10°N, corresponding to the ITCZ in the central/eastern Pacific. While low clouds are ubiquitous across the entire domain, their frequency increases dramatically north of 10°N. Figure SBI.1b shows how the boundary layer deepens with increasing near-surface air temperature along the transect from just east of the subtropical high toward the equator until sufficient instability allows for middle and deep convective clouds. The transition occurs for a surface air temperature near 298 K, consistent with the ascent of an undiluted parcel from the LCL to its level of neutral buoyancy. Figure SBI.2 shows that the frequency of low-level, single-layered marine stratus and stratocumulus from CALIPSO and CloudSat is linearly correlated with the difference in the MSE between air at the midpoint of the inversion below 700 mb, or at the 700 mb level if no inversion exists, and the surface. (Moist static energy is the sum of potential, latent, and sensible energy.) While the difference in MSE tends to be inversely proportional to surface temperature, sea surface temperature is a less ideal predictor of uniform low cloud frequency, as are either the lower-tropospheric dry static stability (Klein and Hartmann 1993) or the estimated inversion strength (Wood and Bretherton 2006). Further details are given in Kubar et al. (2010, manuscript submitted to *J. Climate*).

SNR, the advantages of flying in formation with the variety of sensors on *Aqua* outweighed the advantage of improved SNR with the lidar in a lower orbit. Table 1 lists the measurement requirements originally defined for CALIOP that form the basis for the core CALIOP data products.

CALIPSO uses a PROTEUS spacecraft, developed by Thalès-Alenia and CNES and operated from a satellite operations control center located in Toulouse, France. Instrument commanding and coordination with the A-train constellation are the responsibilities of NASA. Science data are downlinked once per day via X-band

AND STRATOCUMULUS

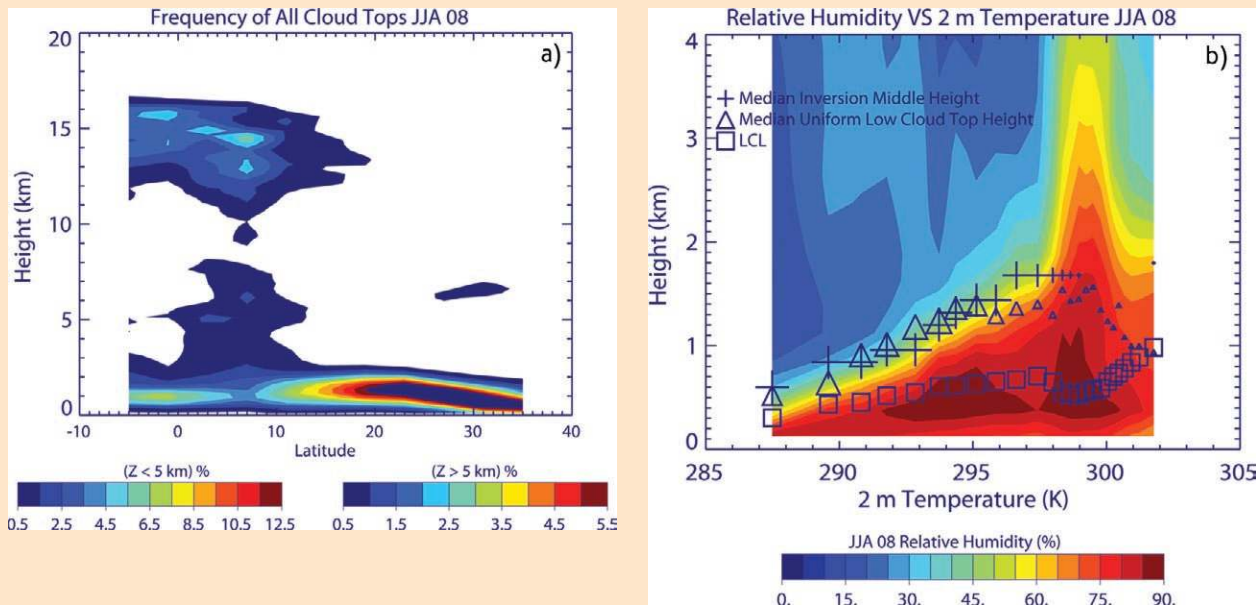


FIG. SBI.1. (a) Cloud-top height and frequency of occurrence with latitude for the 10° -longitude-wide transect centered on the line from 5°S , 180° to 35°N , 120°W . (b) Relative humidity contours, including middle inversion heights (plus signs: relative size indicates relative frequency of the low-level inversion), low cloud-top heights (triangles: relative size indicates relative frequency of single-layered, low-level cloud), and LCLs (squares) with surface air temperature for the transect. Pixels in (b) are for uniform low clouds ($T_{\text{top}} > 273\text{ K}$, $P_{\text{top}} > 500\text{ mb}$), with cloud-top heights determined from merged CALIPSO–CloudSat observations and uniformity based on the MODIS uniformity flag around each CALIPSO–CloudSat footprint. The relative humidity profiles and surface air temperatures were obtained from ECMWF analyses. The observations cover the months of Jun–Aug 2008.

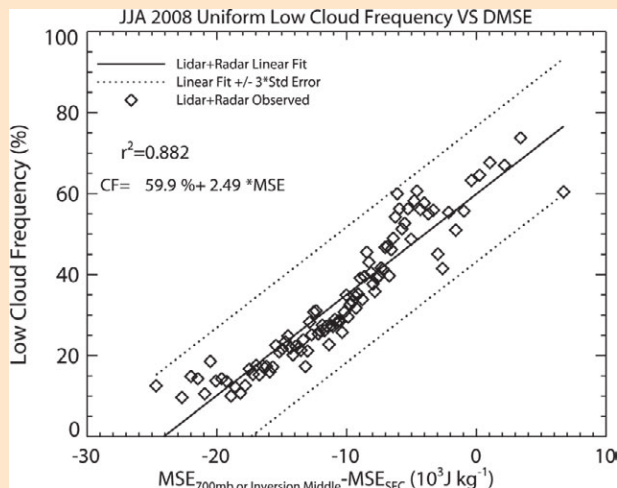


Fig. SBI.2. Uniform, single-layer, low-cloud frequency and difference in the moist static energy between the mid-inversion level, or 700 mb if no inversion exists, and the surface, as deduced from merged CALIPSO, CloudSat, and MODIS observations. Moist static energy is calculated from ECMWF temperature and humidity profiles.

telemetry to commercial ground stations in Alaska and Hawaii. Science data processing and archiving are performed by the NASA LaRC Atmospheric Sciences Data Center. A mirror data site, part of the French ICARE structure, is located in Lille, France, and operated by CNES, the CNRS, the University of Lille, and the Région Nord-Pas de Calais.

TABLE 1. CALIPSO measurement requirements [optical depth, τ ; particulate extinction profile, $\sigma(z)$]. The asterisk indicates 30% uncertainty in backscatter-to-extinction ratio is assumed.

Data product	Measurement capabilities and uncertainties
Aerosols	
Height, thickness	For layers with $\tau > 0.005$
$\tau, \sigma(z)$	$\pm 40\%^*$
Clouds	
Height	For layers with $\tau > 0.01$
Thickness	For layers with $\tau < 5$
$\tau, \sigma(z)$	Within a factor of 2 for $\tau < 5$
Ice/water phase	Layer by layer
Ice cloud emissivity, ϵ	± 0.03
Ice particle size	$\pm 50\%$ for $\epsilon > 0.2$

TABLE 2. Key instrument specifications.

CALIOP	
Wavelength	532, 1064 nm
Polarization	532-nm parallel, perpendicular
Laser energy	110 mJ at each wavelength
Laser repetition rate	20.16 Hz
Laser pulse length	20 ns
Footprint diameter	70 m
Receiver FOV	90 m
Footprint spacing	335 m
WFC	
Wavelength	645 nm
Bandpass	50 nm
FOV/swath	125 m / 61 km
IIR	
Wavelength	8.65, 10.6, 12.05 (μm)
Bandpass	0.6–1 (μm)
FOV/swath	1/61 km
NETD @ 250 K	0.09, 0.14, 0.11 K
Absolute calibration	$< \pm 1$ K

PAYLOAD. The CALIPSO payload consists of the CALIOP lidar and two passive sensors (Fig. 1). Key instrument characteristics are summarized in Table 2. Lidars have been used for atmospheric profiling for many decades and have proven to be ideal for the study of optically thin aerosol and cirrus layers. Figure 2a shows a comparison of simultaneous nighttime backscatter return signals over eastern Maryland from CALIOP and equivalent signals from the NASA Langley Research Center airborne high spectral resolution lidar (Hair et al. 2008) flying along the CALIPSO ground track. Both sets of signals are averaged horizontally over 170 km; however, CALIPSO covers this distance in about 25 s versus 15 min for the HSRL. A weak elevated aerosol layer is seen near 4-km altitude, with stronger scattering below about 2.5 km from tenuous cloud and aerosol within the planetary boundary layer. The clear-sky column optical depth is about 0.5 so the signal is attenuated by a factor of 2–3 by the time it reaches the surface. CALIOP signals are much noisier than those from HSRL because of the smaller signal levels detected from orbit and the shorter averaging time. High backscattering in the lowest 500 m results from averaging returns from a varying surface elevation. Discrepancies below 3 km

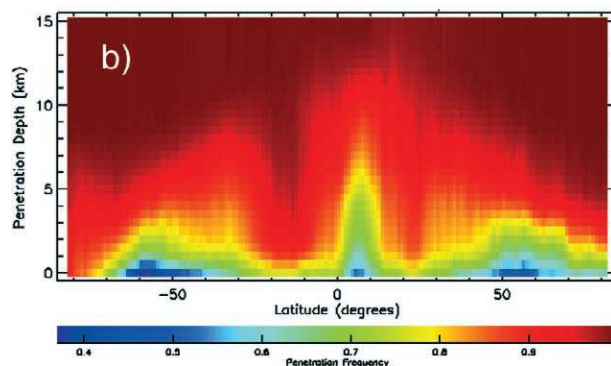
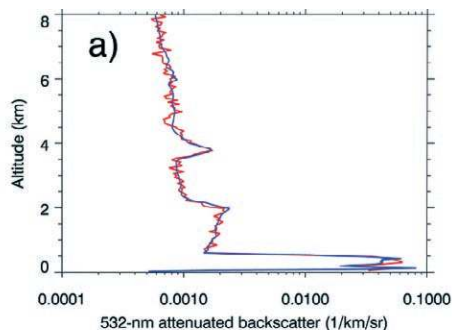


FIG. 2. (a) 532-nm attenuated backscatter profiles from CALIOP (red) and HSRL (blue). (b) Zonal mean CALIOP penetration frequency based on averages of 15 shots (5-km segments) along the orbit.

are likely due to atmospheric dynamics during the time required for the airborne HSRL to cover the 170-km orbit segment.

Most lidars are operated as ground-based systems. Looking up from the ground, the view of the atmosphere is often blocked by low, dense water clouds. Looking down from space provides a view of a larger portion of the atmosphere, as clouds in the upper atmosphere tend to be optically thin. Figure 2b shows the zonal mean frequency with which CALIOP profiles, averaged 5 km along track, penetrate to a given altitude. Despite the prevalence of dense clouds at lower altitudes, 66% of profiles averaged over 5 km reach Earth's surface and 80% penetrate to an altitude of 1.5 km.

Backscatter, depolarization, and attenuated color ratio signatures of a typical scene are shown in Fig. 3. The two CALIOP wavelengths provide a means to distinguish between large and small particles. The backscatter cross section of small aerosol particles is generally larger at 532 than at 1064 nm, but it is independent of wavelength for cloud droplets and ice crystals. However, the absorption of smoke is higher at 532 than at 1064 nm, resulting in a color ratio that increases going into the layer, as can be seen in Fig. 3c near 4°S. Analysis of the spectral backscatter aids the discrimination of cloud and aerosol particles and helps to identify fine- and coarse-mode aerosol.

Outgoing 532-nm laser pulses are linearly polarized, and the receiver measures the polarization of the backscattered return signal. The 180° backscatter from spherical particles retains the polarization of the incident beam, whereas backscatter from nonspherical or irregular particles is depolarized. Thus, depolarization signatures allow discrimination between spherical and nonspherical particles, such as dust and liquid aerosol droplets, or ice crystals and cloud droplets (Sassen 1991; Winker et al. 2007).

The large distance from the satellite to the atmosphere is one of the primary drivers of the lidar design. To provide the best possible measurement sensitivity, CALIOP uses a large receiver telescope and the laser output power was made as large as possible within the limits of spacecraft power. The diameter of the laser footprint was chosen to ensure the beam is eye safe within the atmosphere. In addition to measuring the weak signals from aerosol layers and the molecular atmosphere, CALIOP is also required to accurately measure the strongest cloud returns. Therefore, it was designed with a linear dynamic range spanning many orders of magnitude to encompass the full range of molecular, aerosol, and cloud backscattering. Theoretical estimates of detection sensitivity, in terms of particle extinction coefficient, are shown in Fig. 4. Observation of aerosol and optically thin cloud during daytime is optimized by making the lidar field of view as small as possible and using an etalon with a passband matched to the laser line width to reject the daytime solar background. Figure 4 shows that detection sensitivity for strongly scattering targets, which can be detected without signal averaging, is nearly

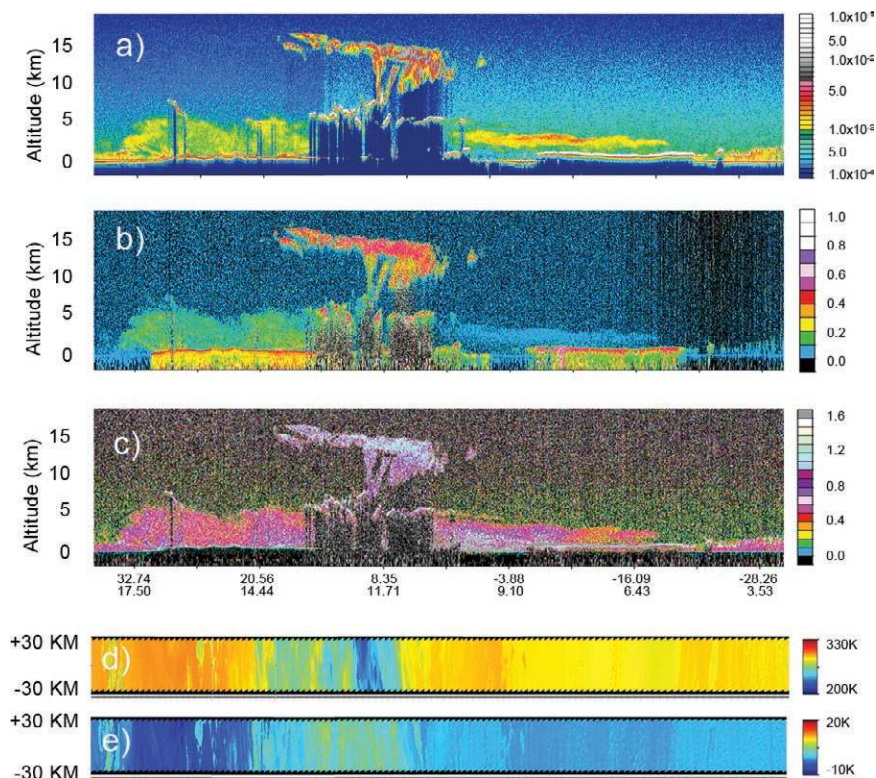


FIG. 3. (a)–(c) CALIOP time–height images and (d), (e) IIR swaths showing dust over (left) the Sahara Desert, (center) tropical cirrus and opaque convective cloud, and (right center) a layer of smoke above a stratus deck. (a) 532-nm backscatter signals; (b) 532-nm depolarization profiles; (c) profiles of attenuated color ratio (the ratio of 1064- and 532-nm backscatter signals); (d) IIR swath, BTs at 12 μm ; and (e) IIR swath, 8–12 μm BT differences.

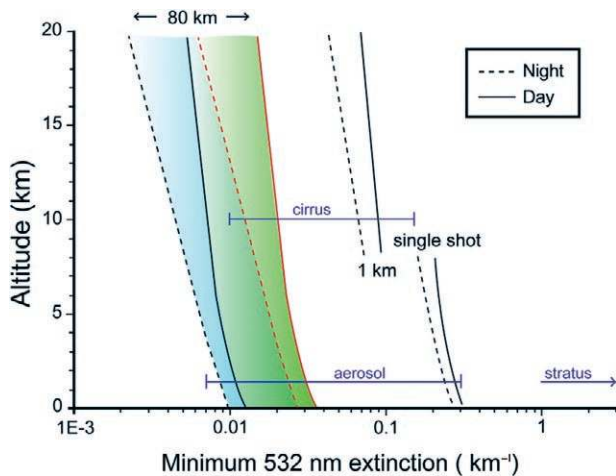


FIG. 4. Theoretical detection sensitivity as a function of altitude for day (solid) and night (dashed) in terms of minimum detectable particulate extinction coefficient (km^{-1}). Sensitivity is shown for clouds at the highest horizontal resolution and for aerosols with horizontal averaging over 80 km. Detection limits are based on the assumption of 90% probability of detection, a vertical resolution of 60 m, and an assumed lidar ratio of 25 sr for clouds. Shaded area corresponds to the range for an assumed aerosol lidar ratio of 25–70 sr (night: blue; day: green). Horizontal lines indicate typical ranges for cirrus and for aerosols and clouds in the atmospheric boundary layer.

the same for day and night, whereas the sensitivity at night is significantly better than during day for weak targets, such as aerosol and thin cirrus layers, which require extensive averaging of backscatter profiles for detection.

The fundamental sampling resolution of CALIOP is determined by the laser pulse repetition rate. Since the spatial variability of clouds and aerosol layers tends to be larger within the atmospheric boundary layer than in the upper atmosphere, data below 8.2 km are downlinked at full resolution. Data above 8.2 km are averaged vertically and horizontally onboard the satellite before downlinking to reduce the required telemetry bandwidth, according to the averaging scheme shown in Table 3. Further information on the instrument and its performance characteristics are given in Winker et al. (2007) and Hunt et al. (2009).

PASSIVE INSTRUMENTS. Two passive sensors were included in the CALIPSO payload to provide atmospheric context around the lidar footprint and to facilitate exploration of combined active–passive retrieval approaches using collocated, simultaneous observations. The IIR and the WFC acquire infrared and visible imagery with swath widths of 61 km centered on the lidar footprint. The spatial resolution of

the WFC is roughly matched to the laser footprint with a pixel FOV of 125 m for pixels within 2.5 km of the lidar footprint and 1 km for the remaining pixels in the swath.

The two passive instruments adopt innovative approaches to provide cost-effective observations. The WFC is based on a commercially available CCD-based star tracker camera with foreoptics modified to provide the required swath and a spectral response matched to MODIS channel 1 at $0.645 \mu\text{m}$. The CCD sensor is temperature controlled to provide radiometric stability and calibrated by comparison of collocated pixels with MODIS (Pitts et al. 2007). The IIR instrument, developed by SODERN and CNES, is based on a 2D microbolometer array (Chomette et al. 2003). The IIR is the first use of an uncooled, temperature-controlled infrared sensor flown in space for radiometric measurements in a science mission. It uses a rotating filter wheel to sequentially measure radiances at three wavelengths in the thermal infrared (Table 2). The chosen wavelengths allow the retrieval of information on ice cloud microphysics, cloud ice/water phase, and mineral dust using an improved version of a differential split-window method first proposed by Inoue (1987). In-flight calibration images are obtained by viewing an onboard blackbody as a warm source and deep space as the cold source (Fig. 1). When pointing at the Earth, the spectral BT distribution observed in the thermal IR is influenced by the presence of mineral dust or cloud ice (Warren 1984; Sokolik et al. 1998). The wavelengths chosen for the IIR allow the retrieval of information on ice cloud microphysics, cloud ice/water phase, and mineral dust. The method for retrieving this information relies on analysis of the variation of radiance with wavelength (Parol et al. 1991), augmented with lidar profile data to provide an accurate reference on cloud and aerosol vertical structure (Chomette et al. 2003). Figure 3 shows coincident lidar and IIR measurements. Variations in BT differences are related to changes in cloud and aerosol microphysical properties as well as

TABLE 3. Spatial resolution of data downlinked from CALIOP.

Altitude range (km)	Horizontal resolution (km)	532-nm vertical resolution (m)	1064-nm vertical resolution (m)
30.1–40.0	5.0	300	—
20.2–30.1	1.67	180	180
8.2–20.2	1.0	60	60
–0.5 to 8.2	0.33	30	60
–2.0 to –0.5	0.33	300	300

TABLE 4. Product summary for (a) CALIOP, version 3 data and (b) IIR and WFC.

(a) Product	Primary parameters	Maximum altitude	Resolution	
			Vertical (m)	Horizontal (km)
DP 1.1 level 1B	532, 532-perpendicular, and 1064-nm attenuated backscatter profiles	40 (km)	Variable (see Table 2)	
DP 2.1A cloud layer products	Base and top height, optical depth, cloud ice/water phase	20	30	1/3, 1, 5
DP 2.1A aerosol layer product	Base and top height, optical depth, aerosol type	30	30	5
DP 2.1B cloud profile product	532-nm backscatter and extinction	20	60	5
DP 2.1C aerosol profile product	532- /1064-nm backscatter and extinction	<20	60	5
		20–30	360	5
DP 2.1D VFM	Cloud mask, ice/water phase, aerosol mask, aerosol type	30	Variable (see Table 2)	

(b) Product	Primary parameters	Spatial resolution
DP 1.2 IIR level 1B	8.65, 10.5, 12- μ m radiances	1 (km)
DP 1.3 WFC level 1B	650-nm radiances	125 m (0–2.5)
		1 km (2.5–30)
DP 2.2A IIR track product	BT, emissivity, ice particle size	1 \times 1
DP 2.2B IIR swath product		1 \times 61

structural properties from atmospheric layers and the surface.

CALIPSO DATA PRODUCTS. Table 4 provides a brief summary of the available CALIPSO data products. CALIOP level 1B data consist of geolocated profiles of calibrated lidar return signals. There are three types of CALIOP level 2 data products: layer products, profile products, and the VFM. Layer products provide layer-integrated or layer-averaged properties for detected aerosol and cloud layers. Profile products provide retrieved extinction and backscatter profiles within these layers. As shown in Table 4a, the data products are provided at various spatial resolutions. Because of the low SNR of the lidar, more averaging is required to detect and retrieve properties for weakly scattering layers than for strongly scattering layers. A multiscale detection and retrieval approach (Winker et al. 2009; Vaughan et al. 2009) was adopted to mitigate the effect of low SNR. Clouds and aerosols are discriminated using a combination of 532-nm backscatter magnitude and attenuated color ratio (Liu et al. 2009). Because information on the spatial locations of cloud and aerosol layers is of fundamental importance, the VFM was developed to provide information on cloud and aerosol locations and type.

Information in the VFM is reported at the resolution of the downlinked data (Table 3).

Level 1 IIR and WFC data consist of calibrated radiances. The IIR track product is based on the IIR pixels coincident with lidar footprints. The IIR swath product uses all the pixels across the IIR swath. All data products—as well as the Data Products Catalog, ATBDs, and other documentation—are available from the ASDC at NASA LaRC (<http://eosweb.larc.nasa.gov>). Further descriptions of the data products can be found in Vaughan et al. (2004), Winker et al. (2009), and the online documentation.

EARLY RESULTS. Despite substantial progress in developing climatologies of global aerosol and cloud properties since the launch of *Terra* (1999) and *Aqua* (2001) (Kaufman et al. 2002; Zhang et al. 2005; Remer et al. 2008), major uncertainties remain. The CALIPSO mission offers a vast improvement in determining the vertical distribution of aerosol and cloud layers and can retrieve aerosol and cloud properties in situations where passive sensors cannot, such as over snow and within multilayered cloud systems.

Observation of aerosol above cloud. The heating effect of absorbing aerosol is increased when the aerosol is

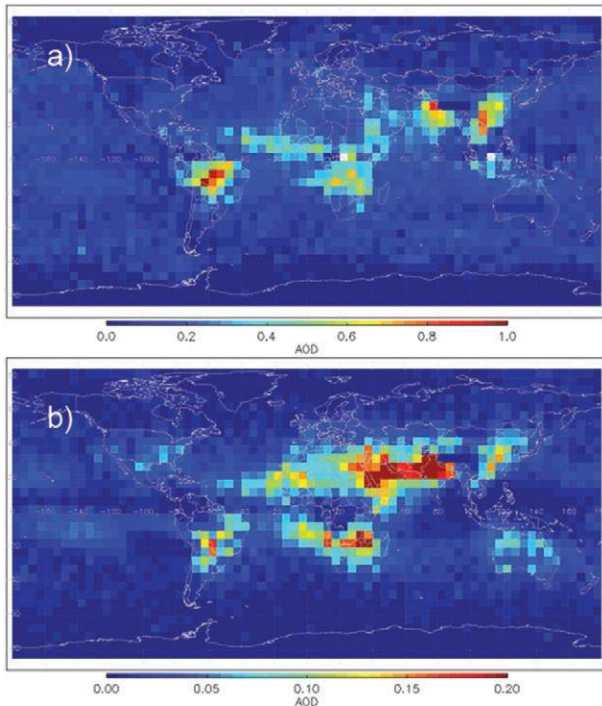


FIG. 5. Mean AOD from CALIOP observations for SON 2007 for (a) clear-sky column AOD and (b) AOD above cloud.

located over a bright surface (Haywood and Shine 1995; Liao and Seinfeld 1998). Consequently, the relative locations of overlapping cloud and absorbing aerosol layers strongly affect the amount of sunlight absorbed. Figure 5 shows seasonal mean aerosol optical depth retrieved from CALIOP returns for clear-sky conditions (Fig. 5a) and for aerosol located above cloud (Fig. 5b; note the change in color-bar scale). Because of the sparse spatial sampling from the nadir-viewing lidar, considerable averaging over space and time is needed to produce meaningful regional averages, such as shown here. The results show the optical depth of aerosol located above cloud can be significant in regions characterized by strong sources of mineral dust, smoke from biomass burning, or pollution. The above-cloud aerosols were previously unobserved, and their effects have been either estimated or neglected in observation-based assessments of aerosol radiative forcing (e.g., Chung et al. 2005). Chand et al. (2009) have used CALIOP observations to estimate the radiative effects of smoke located above low cloud in the southeast Atlantic off the coast of Africa. They find that the warming effect of the smoke is strongly sensitive to the albedo and coverage of the underlying cloud, highlighting the need for collocated cloud and aerosol measurements.

While the latest generation of global climate models predict aerosol optical depths reasonably well (Kinne et al. 2006), model estimates of the vertical distribution of aerosol are unconstrained and vary widely. Model estimates that place too little or too much aerosol above cloud will produce errors in the derived aerosol radiative effects. Profile data from CALIOP offer a more stringent test of models than simple column-integrated aerosol extinction. Figure 6 shows clear-sky mean zonal aerosol extinction retrieved from CALIOP and predicted by the GEOS-5/GOCART model (Colarco et al. 2010). Model data were subsetted to nighttime, clear-sky columns observed by CALIOP. Differences in mean extinction near the surface are related to the strength of model source emissions, but differences aloft indicate stronger vertical and poleward transport of aerosols in the model than observed. Just as models have improved over the last decade by comparing against MODIS and MISR column aerosol optical depth data (Kinne et al. 2006), comparisons of modeled and observed aerosol vertical distribution will lead to further improvements in model performance.

Observations of cloud occurrence and properties.

Cloud climatologies derived from passive satellite sensors differ substantially in the vertical distribution of clouds and in the occurrence of multilayered cloud systems. While differences in cloud properties between the available satellite cloud climatologies are generally smaller than the spread for model-predicted clouds (Zhang et al. 2005), the differences between observations need to be resolved if the observations are to provide useful constraints on model

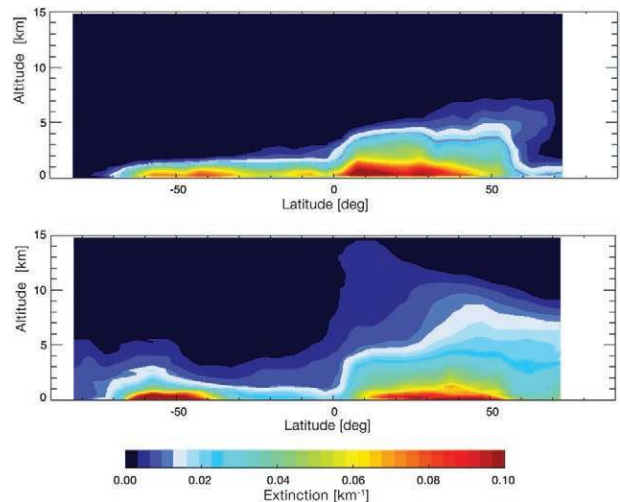


FIG. 6. Mean zonal aerosol extinction for Apr 2008 (a) from CALIPSO observations and (b) as predicted by the GEOS-5/GOCART model.

performance. CALIPSO provides highly resolved vertical profiles of clouds and offers opportunities for improving the metrics used to evaluate models (see “The occurrence of marine stratus and stratocumulus” for more information), while the CloudSat cloud profiling radar has a much greater ability to penetrate cloud. Complementary cloud observations from CALIPSO and CloudSat (see “What is the difference between lidar and cloud profiling radar?” for more information) have been used to produce a merged CALIPSO–CloudSat cloud dataset, providing the first true 3D climatology of global cloud occur-

rence (Mace et al. 2009), and have also been used to produce improved retrievals of ice cloud properties (Delanoë and Hogan 2008). One of the initial applications of the merged CALIPSO–CloudSat cloud product was the assessment of cloud overlap in a form that can be parameterized in global models (Barker 2008). Additionally, lidar instrument simulators have recently been developed to aid in the comparison of CALIOP observations with estimates from global models (e.g., Chepfer et al. 2008).

The satellite cloud climatology used most often in climate model comparisons with observed clouds is

WHAT IS THE DIFFERENCE BETWEEN LIDAR AND CLOUD PROFILING RADAR?

Lidar and radar are similar in concept, emitting pulses of electromagnetic radiation and making time-of-flight measurements of the pulse energy that is scattered back from the atmosphere. But cloud profiling radar operates at wavelengths more than a thousand times longer than lidar wavelengths, giving the two instruments very different capabilities. Electromagnetic waves are scattered most efficiently by particles with sizes similar to the wavelength of the incident electromagnetic radiation. Weather radar uses microwaves with wavelengths on the order of a centimeter that are scattered effectively by precipitation. The CPR on CloudSat uses microwaves with wavelengths on the order of a few millimeters that are scattered efficiently by cloud ice particles. The CPR wavelength is too large to detect aerosol particles, and it has difficulty detecting water clouds composed of small droplets. Lidar uses a laser to generate short pulses of visible or near-infrared light with wavelengths of approximately $1\ \mu\text{m}$ or less, which is scattered efficiently by both cloud and aerosol particles. At wavelengths in the midvisible, even the profile of the molecular atmosphere can be easily measured.

CALIOP is more sensitive to cloud than the CloudSat CPR and can observe tenuous ice clouds and water clouds composed of small droplets that are invisible to CloudSat. On the other hand, the lidar signal is attenuated in dense clouds that the radar signals

penetrate easily. Consequently, CPR and CALIOP provide complementary measurements of clouds. Together they have provided the first global observations of the vertical distribution of cloud (Mace et al. 2009). Because the laser pulse is much shorter than the radar pulse, CALIOP has much higher vertical resolution (30 m) than the CloudSat CPR (500 m) and is able to profile down to Earth’s surface, whereas the CPR loses sensitivity to cloud detection in the lowest 500 m of the atmosphere.

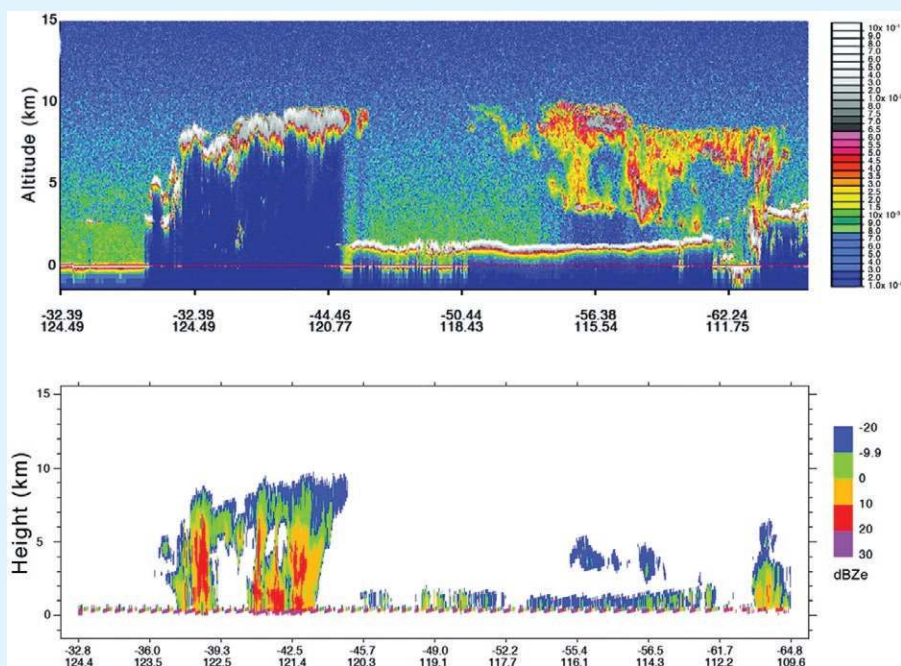


FIG. SB2. The complementary capabilities of the CALIOP (top) and CloudSat CPR (bottom) are illustrated by these coincident observations. The dense cores of storm clouds over the Southern Ocean are seen in CPR data near 40°S, but CPR detects only the denser portions of upper-troposphere ice clouds. CALIOP observes optically thin ice clouds but is unable to penetrate the dense core of the storm system. Owing to a combination of low altitudes and relatively small droplet sizes, low-level marine stratus goes undetected by the CPR but is detected clearly by CALIOP. CPR detects drizzle underneath the stratus, however.

the multidecadal ISCCP dataset (Rossow and Schiffer 1999). Figure 7 compares cloud occurrence for high clouds (top heights greater than 6.5 km or 440 mb), middle clouds (top heights between 3.25 and 6.5 km, or between 680 and 440 mb), and low clouds (top heights less than 3.25 km or 680 mb) from the ISCCP IR-only product and from CALIOP. The geographic pattern for the occurrence of low-level cloud from CALIOP and ISCCP is similar, except in the Southern Ocean, where CALIOP is able to detect a significant amount of low cloud located beneath higher cloud layers. Owing partly to its higher sensitivity and smaller instantaneous field of view (70 m compared with 4–10 km for ISCCP), CALIOP shows higher cloud occurrences in the stratus decks in the eastern Pacific and Atlantic Oceans. CALIOP provides more reliable cloud detection in the polar regions, where passive cloud retrievals are notoriously difficult. As might be expected, greater differences arise for upper-level clouds. Much of the high cloud observed by CALIOP is optically thin and is undetected in the ISCCP IR-only product. The ISCCP occurrence of high cloud is also under-reported because the heights of semitransparent clouds derived from 11- μm radiances are often biased low (Jin et al. 1996; Chang

and Li 2005). While the mean global occurrence of middle-level cloud is similar for the two datasets, again significant regional differences arise, notably over continents, in the Southern Ocean, and to the west of the Peruvian coast.

CALIOP cloud data have been widely used to validate and characterize passive cloud retrievals (e.g. Weisz et al. 2007; Kahn et al. 2008; Stubenrauch et al. 2008; Minnis et al. 2008; Hayes et al. 2010). A-train formation flying has produced a multisensor dataset with orders of magnitude more instantaneous collocated measurements than available from overpasses of ground sites, making possible for the first time large ensembles for characterizing the errors in passive retrieval methods. For example, Holz et al. (2008) found the heights of marine stratus decks in MODIS collection 5 were systematically overestimated by 1–2 km. The cause of the bias was identified, and a modified MODIS algorithm has been introduced to reduce the bias.

Thin cirrus. As was noted earlier, the properties of thin cirrus, particularly when overlapped with low-level clouds, pose a challenge for passive remote sensing and consequently for determining the

effects of changes in cirrus on climate. CALIPSO offers a suite of new tools that will vastly improve the characterization of optically thin cirrus. Cooper et al. (2003) showed that accurate knowledge of cloud boundaries can significantly improve infrared retrievals of the properties of semitransparent clouds. Retrievals of cloud emissivity and particle size from the IIR instrument use lidar profiles to identify multilayered cloud scenes and to facilitate the identification of clear or cloudy air beneath upper-level clouds to accurately estimate infrared radiances (Chomette et al. 2003).

Figure 8 shows global estimates of the emissivities of high-altitude semitransparent cloud (with tops higher than 7 km) using a retrieval that

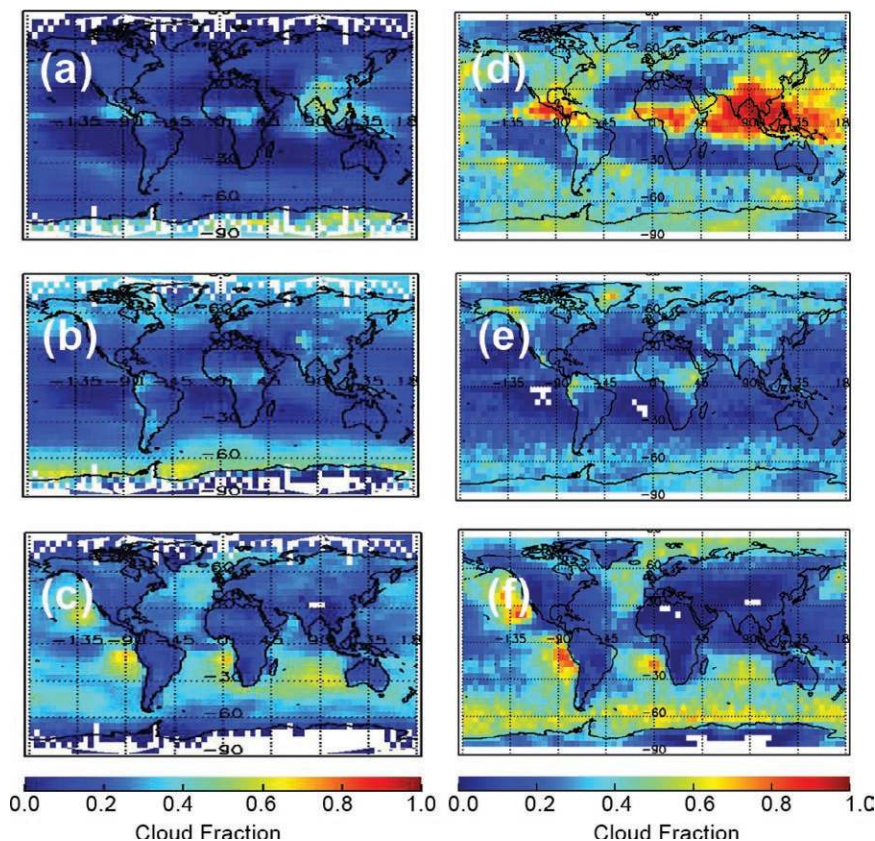


FIG. 7. Mean cloud occurrence for Jun–Aug 2007 of (a)–(c) ISCCP IR high, middle, and low cloud; and (d)–(f) CALIOP high, middle, and low cloud.

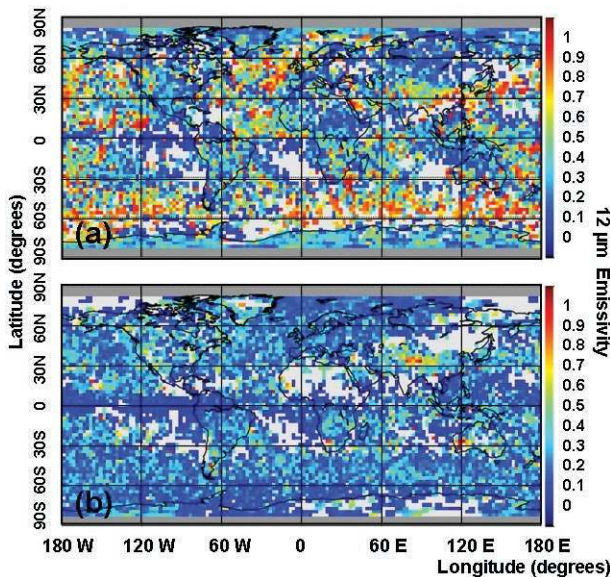


FIG. 8. Mean 12- μm emissivities of semitransparent upper-level clouds for Jan 2008 from combined IIR-CALIOP retrievals, day and night of (a) single-layer cirrus clouds and (b) located above opaque low-level clouds.

combines infrared and lidar profile observations. Scenes were identified using CALIOP profile data, and the IIR retrievals were extrapolated from the lidar track to the limits of the 60-km IIR swath. White areas correspond to scene types other than high-altitude clouds. Figure 8 shows emissivities for semitransparent high clouds occurring alone (top panel) and above low-altitude opaque cloud (bottom panel). Such clouds are seen to be nearly ubiquitous outside areas of deep convection. Although some regional patterns are clearly visible, the largest emissivities are observed over the ocean and are more frequent in the Southern Hemisphere. These unique retrievals of thin, semitransparent clouds can be combined with independently retrieved cloud visible optical depths from CALIOP to evaluate the radiative properties and the climatic effect of these thin clouds.

Of course, the properties of thin cirrus are greatly influenced by the properties of the ice crystals that constitute the cloud, their habits and sizes, and their possible formation from the nucleation of supercooled water droplets. CALIOP depolarization profiles (Hu et al. 2009) now allow vertically resolved retrievals of cloud ice/water phase as shown in Fig. 9. Such observations provide a new tool for evaluating climate model performance.

Effects of thin cirrus on the TTL. The TTL is a transition region between the upper troposphere and the lower stratosphere in the tropics (Fueglistaler et al. 2009). The base of the TTL is usually defined as the level of

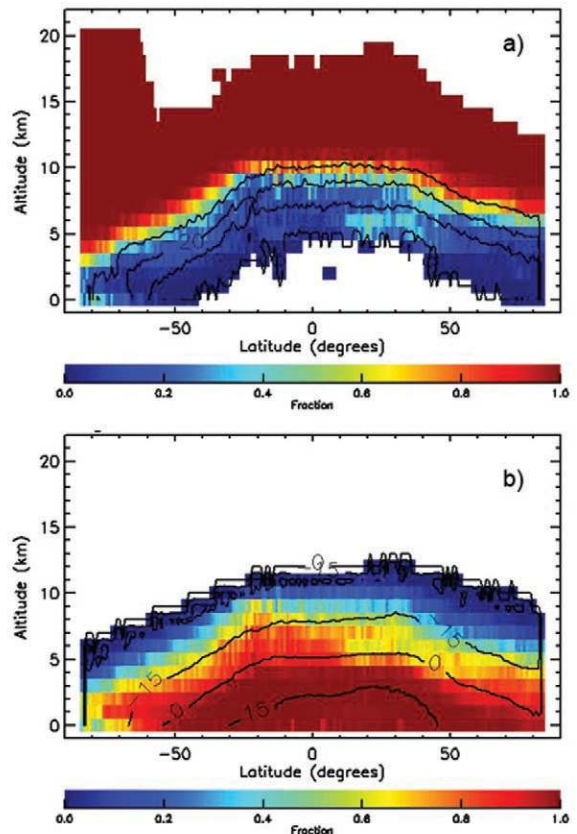


FIG. 9. Zonal mean fraction of ice cloud and water cloud for Aug 2007. (a) contours = -30° , -20° , -10° , 0°C ; (b) contours = -30° , -15° , 0° , $+15^{\circ}\text{C}$.

zero net radiative heating, the dividing line between ascending and descending air parcels at approximately 14–15 km (e.g., Gettelman et al. 2004; Corti et al. 2005). The top of the TTL is defined as the height where the upward mass flux decreases to that of the Brewer–Dobson circulation in the lower stratosphere. CALIOP cloud observations together with a vertical mass flux analysis were used to establish the top of the TTL at about 70 mB (~ 18.5 km; Fu et al. 2007).

The radiative energy budget within the TTL is critical in determining the mass exchange between the troposphere and stratosphere and the water balance of the stratosphere. The radiative effects of optically thin cirrus in the TTL are thought to greatly influence troposphere–stratosphere exchange (Hartmann et al. 2001; Corti et al. 2005). Thin cirrus located above deep convective clouds have a cooling effect, whereas thin cirrus heated by radiation in the infrared window emitted by low-level clouds and the surface have a warming effect. Most of the cloud layers observed in the TTL by CALIOP are optically thin, with optical depths less than 0.3 and thus they

are largely undetected by passive satellite sensors or by the CloudSat radar. Feldman et al. (2008) used data from CALIOP and CloudSat to study the effects of this thin TTL cirrus on the level of zero net radiative heating. Inclusion of optically thin cirrus observed by CALIOP but not observed by CloudSat lowered the estimated level of zero net radiative heating, thereby increasing the thickness of the TTL and influencing the exchange between the TTL and the lower stratosphere. In addition, one of the most robust responses of the atmospheric circulation to the increase of greenhouse gases is the strengthening of the Brewer–Dobson circulation (Butchart et al. 2006; Fu et al. 2010). Changes in the tropical tropopause temperature are largely controlled by changes in the Brewer–Dobson circulation (Yulaeva et al. 1994). Any temperature changes are likely to affect the thin cirrus in the region, thereby giving rise to a response to the increase of greenhouse gases that alter the energy budget of the troposphere–surface system. Multiyear CALIPSO observations of thin cirrus in the TTL will provide an unprecedented opportunity to characterize this cloud–climate feedback.

OPPORTUNITIES, PROSPECTS, AND EMERGING APPLICATIONS. Data from CALIPSO are still relatively new and are just beginning to be used extensively by the scientific community. In this section several areas of active research are highlighted where CALIPSO observations are expected to make significant contributions in the near future.

- i) Broadband radiative fluxes at the TOA are accurately measured using observations from the CERES and MODIS instruments flying on *Terra* and *Aqua* (Wielicki et al. 1995; Loeb et al. 2009). Radiative fluxes at the surface and within the atmosphere, however, depend strongly on the vertical profile of clouds. CALIOP and CloudSat profiles are now being combined with *Aqua* MODIS and CERES data by several research groups to provide improved, observation-based estimates of surface radiative fluxes and atmospheric heating profiles.
- ii) Data assimilation provides detailed insight into discrepancies between observations and models and represents a powerful approach for model improvement. The use of 4DVAR in the assimilation of ground-based lidar network data has recently been demonstrated (Hara et al. 2009) and work is underway in several modeling groups to develop techniques to assimilate CALIOP profiles.

- iii) The retrieval of ocean surface roughness from spaceborne lidar observations was demonstrated using observations from LITE (Menzies et al. 1998), but CALIOP data have allowed progress in the analysis of ocean surface and subsurface signals (Hu et al. 2008). Recent work combining CALIOP, CloudSat, and passive microwave measurements points toward the use of lidar ocean surface returns to improve the retrievals of column aerosol optical depth and extinction profiles (Josset et al. 2008).
- iv) Satellite observations of column aerosol burdens are beginning to be used in air quality forecasting (Al-Saadi et al. 2005) but significant uncertainties arise in using column measurements to estimate concentrations at the surface. CALIPSO profiles are being explored as a means to improving the integration of satellite column measurements with measurements from existing surface networks.

CONCLUSIONS. The CALIPSO mission represents a successful cooperative effort between NASA and CNES and has provided the first multiyear global dataset of lidar aerosol and cloud profiles. CALIOP active profiling in conjunction with A-train and CALIPSO passive observations are opening new fields of investigation into the role of aerosol and clouds in the climate system. Quantitative assessments of passive sensor performance using CALIOP observations have led to improvements in operational retrievals, and a variety of synergistic retrievals of aerosol and cloud properties have been explored. The international community is still learning how to use this new dataset, but CALIPSO observations have already provided new insights into characteristics of aerosol and cloud that are critical to understanding their role in the climate system.

Carrying the APS, the Glory satellite (Mishchenko et al. 2007) is scheduled to join the A-train in late 2010. Measurements of polarized spectral radiances from APS with coincident CALIOP profiles will provide opportunities to explore new retrieval approaches and serve as a pathfinder for advanced missions, as suggested by the National Research Council's Decadal Survey (NRC 2007), and now in the planning stages. In the meantime, the European Space Agency is developing two satellite missions carrying advanced lidars: the ADM-Aeolus, to be launched in 2011, and EarthCARE. These missions can continue the record of aerosol and cloud profiles begun by CALIPSO, potentially leading to the multidecadal observational record needed to characterize climate trends.

ACKNOWLEDGMENTS. This work was funded by the National Aeronautics and Space Administration, Centre National d'Etudes Spatiales, and Centre National de la Recherche Scientifique/Institut National des Sciences de l'Univers. We would like to acknowledge the support and successful cooperation of NASA and CNES in the development and operation of CALIPSO and the advocacy of Gérard Mégie for the mission. We thank Bill Hunt and the team at Ball Aerospace for CALIOP and payload integration; the teams at SODERN and Thales Alenia Space for the IIR and platform integration, respectively; the operations teams at NASA and CNES; and the support of the ASDC and ICARE data centers, who all made essential contributions to the success of the CALIPSO mission. The work described in "The occurrence of marine stratus and stratocumulus" was carried out by T. Kubar in collaboration with D. E. Waliser and J.-L. F. Li at the Jet Propulsion Laboratory, California Institute of Technology, under a contract with the National Aeronautics and Space Administration. We thank Brian Getzewitch for the analyses of cloud statistics presented here. Lastly, we would like to acknowledge Chieko Kittaka's many contributions to the CALIPSO team. She is sorely missed.

REFERENCES

- Ackerman, A. S., O. B. Toon, D. E. Stevens, A. J. Heymsfield, V. Ramanathan, and E. J. Welton, 2000: Reduction of tropical cloudiness by soot. *Science*, **288**, 1042–1047.
- Al-Saadi, J., and Coauthors, 2005: Improving national air quality forecasts with satellite aerosol observations. *Bull. Amer. Meteor. Soc.*, **86**, 1249–1261.
- Barker, H. W., 2008: Overlap of fractional cloud for radiation calculations in GCMs: A global analysis using CloudSat and CALIPSO data. *J. Geophys. Res.*, **113**, D00A01, doi:10.1029/2007JD009677.
- Bellouin, N., A. Jones, J. Haywood, and S. A. Christopher, 2008: Updated estimate of aerosol direct radiative forcing from satellite observations and comparison against the Hadley Centre climate model. *J. Geophys. Res.*, **113**, D10205, doi:10.1029/2007JD009385.
- Bony, S., and Dufresne, J.-L., 2005: Marine boundary layer clouds at the heart of tropical cloud feedback uncertainties in climate models. *Geophys. Res. Lett.*, **32**, L20806, doi:10.1029/2005GL023851.
- Butchart, N., and Coauthors, 2006: Simulations of anthropogenic change in the strength of the Brewer-Dobson circulation. *Climate Dyn.*, **27**, 727–741, doi:10.1007/s00382-006-0162-4.
- Cess, R. D., and Coauthors, 1990: Intercomparison and interpretation of climate feedback processes in 19 atmospheric general circulation models. *J. Geophys. Res.*, **95**, 16601–16615.
- Chand, D., R. Wood, T. L. Anderson, S. K. Satheesh, and R. J. Charlson, 2009: Satellite-derived direct radiative effect of aerosols dependent on cloud cover. *Nat. Geosci.*, **2**, 181–184, doi:10.1038/ngeo437.
- Chang, F.-L., and Z. Li, 2005: A near-global climatology of single-layer and overlapped clouds and their optical properties retrieved from Terra/MODIS data using a new algorithm. *J. Climate*, **18**, 4752–4771.
- Charlson, R. J., S. E. Schwartz, J. M. Hales, R. D. Cess, J. A. Coakley, J. E. Hansen, and D. J. Hoffman, 1992: Climate forcing by anthropogenic aerosols. *Science*, **255**, 423–430.
- , A. S. Ackerman, F. A.-M. Bender, T. L. Anderson, and Z. Liu, 2007: On the climate forcing consequences of the albedo continuum between cloudy and clear air. *Tellus*, **59B**, 715–727.
- Chepfer, H., S. Bony, D. M. Winker, M. Chiriaco, J.-L. Dufresne, and G. Sèze, 2008: Use of CALIPSO lidar observations to evaluate the cloudiness simulated by a climate model. *Geophys. Res. Lett.*, **35**, L15704, doi:10.1029/2008GL034207.
- Chomette, O., and Coauthors, 2003: Retrieval of cloud emissivity and particle size in the frame of the CALIPSO mission. IGARSS 2003: Learning from Earth's Shapes and Sizes, Vol. 3, IEEE, 1520–1522.
- Chung, C. E., V. Ramanathan, D. Kim, and I. A. Podgorny, 2005: Global anthropogenic aerosol direct forcing derived from satellite and ground-based observations. *J. Geophys. Res.*, **110**, D24207, doi:10.1029/2005JD006356.
- Colarco, P., A. da Silva, M. Chin, and T. Diehl, 2010: Online simulations of global aerosol distributions in the NASA GEOS-4 model and comparisons to satellite and ground-based aerosol optical depth. *J. Geophys. Res.*, **115**, D14207, doi:10.1029/2009JD012820.
- Cooper, S. J., T. S. L'Ecuyer, and G. L. Stephens, 2003: The impact of explicit cloud boundary information on ice cloud microphysical property retrievals from infrared radiances. *J. Geophys. Res.*, **108**, 4107, doi:10.1029/2002JD002611.
- Corti, T., B. P. Luo, T. Peter, H. Vömel, and Q. Fu, 2005: Mean radiative energy balance and vertical mass fluxes in the equatorial upper troposphere and lower stratosphere. *Geophys. Res. Lett.*, **32**, L06802, doi:10.1029/2004GL021889.
- Delanoë, J., and R. J. Hogan, 2008: A variational scheme for retrieving ice cloud properties from combined radar, lidar, and infrared radiometer. *J. Geophys. Res.*, **113**, D07204, doi:10.1029/2007JD009000.
- Doutriaux-Boucher, M., and J. Qaas, 2004: Evaluation of cloud thermodynamic phase parameterizations in the LMDZ GCM by using POLDER

- satellite data. *Geophys. Res. Lett.*, **31**, L06126, doi:10.1029/2003GL019095.
- Dufresne, J.-L., and S. Bony, 2008: An assessment of the primary sources of spread of global warming estimates from coupled atmosphere–ocean models. *J. Climate*, **21**, 5135–5144.
- Feldman, D. R., T. S. L'Ecuyer, K. N. Liou, and Y. L. Yung, 2008: Remote sensing of tropical tropopause layer radiation balance using A-train measurements. *J. Geophys. Res.*, **113**, D21113, doi:10.1029/2008JD010158.
- Fowler, L. D., and D. A. Randall, 1996: Liquid and ice cloud microphysics in the CSU general circulation model. Part III: Sensitivity to modeling assumptions. *J. Climate*, **9**, 561–586.
- Fu, Q., Y. Hu, and Q. Yang, 2007: Identifying the top of the tropical tropopause layer from vertical mass flux analysis and CALIPSO lidar cloud observations. *Geophys. Res. Lett.*, **34**, L14813, doi:10.1029/2007GL030099.
- , S. Solomon, and P. Lin, 2010: On the seasonal dependence of tropical lower-stratospheric temperature trends. *Atmos. Chem. Phys.*, **10**, 2643–2653.
- Fueglistaler, S., A. E. Dessler, T. J. Dunkerton, I. Folkins, Q. Fu, and P. W. Mote, 2009: Tropical tropopause layer. *Rev. Geophys.*, **47**, RG1004, doi:10.1029/2008RG000267.
- Gottelman, A., P. M. de F. Forster, M. Fujiwara, Q. Fu, H. Vömel, L. K. Gohar, C. Johanson, and M. Ammerman, 2004: Radiation balance of the tropical tropopause layer. *J. Geophys. Res.*, **109**, D07103, doi:10.1029/2003JD004190.
- Hair, J. W., and Coauthors, 2008: Airborne High Spectral Resolution Lidar for profiling aerosol optical properties. *Appl. Opt.*, **47**, 6734–6752.
- Hara, Y., K. Yumimoto, I. Uno, A. Shimizu, N. Sugimoto, Z. Liu, and D. M. Winker, 2009: Asian dust outflow in the PBL and free atmosphere retrieved by NASA CALIPSO and an assimilated dust transport model. *Atmos. Chem. Phys.*, **9**, 1227–1239.
- Hartmann, D. L., M. E. Ockert-Bell, and M. L. Michelson, 1992: The effect of cloud type on earth's energy balance: Global analysis. *J. Climate*, **5**, 1281–1304.
- , J. R. Holton, and Q. Fu, 2001: The heat balance of the tropical tropopause, cirrus, and stratospheric dehydration. *Geophys. Res. Lett.*, **28**, 1969–1972.
- Hayes, C. R., J. A. Coakley Jr., and W. R. Tahnk, 2010: Relationships among the properties of marine stratocumulus derived from collocated CALIPSO and MODIS observations. *J. Geophys. Res.*, **115**, D00H17, doi:10.1029/2009JD012046.
- Haywood, J. M., and K. P. Shine, 1995: The effect of anthropogenic sulfate and soot aerosol on the clear sky planetary radiation budget. *Geophys. Res. Lett.*, **22**, 603–606.
- Holz, R., S. Ackerman, F. Nagle, R. Frey, S. Dutcher, R. Kuehn, M. Vaughan, and B. Baum, 2008: Global Moderate Imaging Spectroradiometer (MODIS) cloud detection and height evaluation using CALIOP. *J. Geophys. Res.*, **113**, D00A19, doi:10.1029/2008JD009837.
- Hu, Y., and Coauthors, 2008: Sea surface wind speed estimation from space-based lidar measurements. *Atmos. Chem. Phys.*, **8**, 3593–3601.
- , and Coauthors, 2009: CALIPSO/CALIOP cloud phase discrimination algorithm. *J. Atmos. Oceanic Technol.*, **26**, 2293–2309.
- Hunt, W. H., D. M. Winker, M. A. Vaughan, K. A. Powell, P. L. Lucker, and C. Weimer, 2009: CALIPSO lidar description and performance assessment. *J. Atmos. Oceanic Technol.*, **26**, 1214–1228.
- Inoue, T., 1987: A cloud type classification with NOAA-7 split-window measurements. *J. Geophys. Res.*, **92**, 3991–4000.
- Jin, Y., W. B. Rossow, and D. P. Wylie, 1996: Comparison of the climatologies of high-level clouds from HIRS and ISCCP. *J. Climate*, **9**, 2850–2879.
- Josset, D., J. Pelon, A. Protat, and C. Flamant, 2008: New approach to determine aerosol optical depth from combined CALIPSO and CloudSat ocean surface echoes. *Geophys. Res. Lett.*, **35**, L10805, doi:10.1029/2008GL033442.
- Kahn, B. H., and Coauthors, 2008: Cloud type comparisons of AIRS, CloudSat, and CALIPSO cloud height and amount. *Atmos. Chem. Phys.*, **8**, 1231–1248.
- Kaufman, Y., D. Tanre, and O. Boucher, 2002: A satellite view of aerosols in the climate system. *Nature*, **419**, 215–223.
- , I. Koren, L. A. Remer, D. Rosenfeld, and Y. Rudich, 2005: The effect of smoke, dust, and pollution aerosol on shallow cloud development over the Atlantic ocean. *Proc. Natl. Acad. Sci. USA*, **102**, 11 207–11 212, doi:10.1073/pnas.0505191102.
- King, M. D., Y. J. Kaufman, D. Tanré, and T. Nakajima, 1999: Remote sensing of tropospheric aerosols from space: Past, present, and future. *Bull. Amer. Meteor. Soc.*, **80**, 2229–2259.
- Kinne, S., and Coauthors, 2006: An AeroCom initial assessment—Optical properties in aerosol component modules of global models. *Atmos. Chem. Phys.*, **6**, 1815–1834.
- Klein, S. A., and D. L. Hartmann, 1993: The seasonal cycle of low stratiform clouds. *J. Climate*, **6**, 1587–1606.
- Li, Z.-X., and H. Le Treut, 1992: Cloud-radiation feedbacks in a general circulation model and their de-

- pendence on cloud modelling assumptions. *Climate Dyn.*, **7**, 133–139.
- Liao, H., and J. H. Seinfeld, 1998: Effect of clouds on direct aerosol radiative forcing of climate. *J. Geophys. Res.*, **103**, 3781–3788.
- Liu, Z., M. A. Vaughan, D. M. Winker, C. Kittaka, B. J. Getzewich, R. E. Kuehn, A. Omar, K. Powell, C. R. Trepte, and C. A. Hostetler, 2009: The CALIPSO lidar cloud and aerosol discrimination: Version 2 algorithm and initial assessment of performance. *J. Atmos. Oceanic Technol.*, **26**, 1198–1213.
- Loeb, N. G., B. A. Wielicki, D. R. Doelling, G. L. Smith, D. F. Keyes, S. Kato, N. Manalo-Smith, and T. Wong, 2009: Toward optimal closure of the earth's top-of-atmosphere radiation budget. *J. Climate*, **22**, 748–766.
- Lohmann, U., and J. Feichter, 2005: Global indirect aerosol effects: A review. *Atmos. Chem. Phys.*, **5**, 715–737.
- Mace, G. G., Q. Zhang, M. Vaughan, R. Marchand, G. Stephens, C. Trepte, and D. Winker, 2009: A description of hydrometeor layer occurrence statistics derived from the first year of merged Cloudsat and CALIPSO data. *J. Geophys. Res.*, **114**, D00A26, doi:10.1029/2007JD009755.
- Marshak, A., G. Wen, J. A. Coakley Jr., L. A. Remer, N. G. Loeb, and R. F. Cahalan, 2008: A simple model for the cloud adjacency effect and the apparent bluing of aerosols near clouds. *J. Geophys. Res.*, **113**, D14S17, doi:10.1029/2007JD009196.
- Matheson, M. A., J. A. Coakley Jr., and W. R. Tahnk, 2005: Aerosol and cloud property relationships for summertime stratiform clouds in the northeastern Atlantic from Advanced Very High Resolution observations. *J. Geophys. Res.*, **110**, D24204, doi:10.1029/2005JD006165.
- , —, and —, 2006: Effects of threshold retrievals on estimates of the aerosol indirect radiative forcing. *Geophys. Res. Lett.*, **33**, L07705, doi:10.1029/2005GL025614.
- Menzies, R. T., D. M. Tratt, and W. H. Hunt, 1998: Lidar in-space technology experiment measurements of sea surface directional reflectance and the link to surface wind speed. *Appl. Opt.*, **37**, 5550–5559.
- Minnis, P., C. R. Yost, S. Sun-Mack, and Y. Chen, 2008: Estimating the top altitude of optically thick ice clouds from thermal infrared satellite observations using CALIPSO data. *Geophys. Res. Lett.*, **35**, L12801, doi:10.1029/2008GL033947.
- Mishchenko, M. I., and Coauthors, 2007: Accurate monitoring of terrestrial aerosols and total solar irradiance: Introducing the Glory mission. *Bull. Amer. Meteor. Soc.*, **88**, 677–691.
- Nakajima, T., A. Higurashi, K. Kawamoto, and J. E. Penner, 2001: A possible correlation between satellite-derived cloud and aerosol microphysical parameters. *Geophys. Res. Lett.*, **28**, 1171–1174.
- NRC, 2007: *Earth Science and Applications from Space: National Imperatives for the Next Decade and Beyond*. The National Academies Press, 428 pp.
- Parol, F., J. C. Buriez, G. Brogniez, and Y. Fouquart, 1991: Information content of AVHRR channels 4 and 5 with respect to the effective radius of cirrus cloud particles. *J. Appl. Meteor.*, **30**, 973–984.
- Penner, J. E., S. Y. Zhang, and C. C. Chuang, 2003: Soot and smoke aerosol may not warm climate. *J. Geophys. Res.*, **108**, 4657, doi:10.1029/2003JD003409.
- Pitts, M. C., L. W. Thomason, Y. Hu, and D. M. Winker, 2007: An assessment of the on-orbit performance of the CALIPSO wide field camera. Remote Sensing of Clouds and the Atmosphere XII, A. Comerón et al., Eds., International Society for Optical Engineering (SPIE Proceedings, Vol. 6745), doi:10.1117/12.737377.
- Platnick, S., M. D. King, S. A. Ackerman, W. P. Menzel, B. A. Baum, J. C. Riédi, and R. A. Frey, 2003: The MODIS cloud products: Algorithms and examples from Terra. *IEEE Trans. Geosci. Remote Sens.*, **41**, 459–473.
- Quijano, A. L., I. N. Sokolik, and O. B. Toon, 2000: Radiative heating rates and direct radiative forcing by mineral dust in cloudy atmospheric conditions. *J. Geophys. Res.*, **105**, 12207–12219.
- Randall, D. A., Harshvardhan, D. A. Dazlich, and T. G. Corsetti, 1989: Interactions among radiation, convection, and large-scale dynamics in a general circulation model. *J. Atmos. Sci.*, **46**, 1943–1970.
- Remer, L. A., and Coauthors, 2008: Global aerosol climatology from the MODIS satellite sensors. *J. Geophys. Res.*, **113**, D14S07, doi:10.1029/2007JD009661.
- Rossow, W. B., and R. A. Schiffer, 1999: Advances in understanding clouds from ISCCP. *Bull. Amer. Meteor. Soc.*, **80**, 2261–2287.
- Sassen, K., 1991: The polarization lidar technique for cloud research: A review and current assessment. *Bull. Amer. Meteor. Soc.*, **72**, 1848–1866.
- Sekiguchi, M., T. Nakajima, K. Suzuki, K. Kawamoto, A. Higurashi, D. Rosenfeld, I. Sano, S. Mukai, 2003: A study of the direct and indirect effects of aerosols using global satellite data sets of aerosol and cloud parameters. *J. Geophys. Res.*, **108**, 4699, doi:10.1029/2002JD003359.
- Sokolik, I. N., O. B. Toon, and R. W. Bergstrom, 1998: Modelling the radiative characteristics of airborne mineral aerosols at infrared wavelengths. *J. Geophys. Res.*, **103**, 8813–8826.

- Solomon, S., D. Qin, M. Maning, Z. Chen, M. Marquis, K. B. Averyt, M. Tignor, and H. L. Miller, Eds., 2007: *Climate Change 2007: The Physical Science Basis*. Cambridge University Press, 996 pp.
- Stephens, G. L., and Coauthors, 2002: The CloudSat mission and the A-train: A new dimension of space-based observations of clouds and precipitation. *Bull. Amer. Meteor. Soc.*, **83**, 1771–1790.
- Stubenrauch, C. J., S. Cros, N. Lamquin, R. Amante, A. Chédin, C. Crevoisier, and N. A. Scott, 2008: Cloud properties from Atmospheric Infrared Sounder and evaluation with Cloud-Aerosol Lidar and Infrared Pathfinder Satellite Observations. *J. Geophys. Res.*, **113**, D00A10, doi:10.1029/2008JD009928.
- Sun, Z., and K. P. Shine, 1995: Parameterization of ice cloud radiative properties and its application to the potential climatic importance of mixed-phased clouds. *J. Climate*, **8**, 1874–1888.
- Tackett, J. L., and L. Di Girolamo, 2009: Enhanced aerosol backscatter adjacent to tropical trade wind clouds revealed by satellite-based lidar. *Geophys. Res. Lett.*, **36**, L14804, doi:10.1029/2009GL039264.
- Trenberth, K. E., J. T. Fasullo, and J. Kiehl, 2009: Earth's global energy budget. *Bull. Amer. Meteor. Soc.*, **90**, 311–323.
- Tsushima, Y., and Coauthors, 2006: Importance of the mixed-phase cloud distribution in the control climate for assessing the response of clouds to carbon dioxide increase: A multi-model study. *Climate Dyn.*, **27**, 113–126.
- Twohy, C. H., J. A. Coakley Jr., and W. R. Tahnk, 2009: Effect of changes in relative humidity on aerosol scattering near clouds. *J. Geophys. Res.*, **114**, D05205, doi:10.1029/2008JD010991.
- Twomey, S. A., 1977: The influence of pollution on the shortwave albedo of clouds. *J. Atmos. Sci.*, **34**, 1149–1152.
- Vaughan, M., S. Young, D. Winker, K. Powell, A. Omar, Z. Liu, Y. Hu, and C. Hostetler 2004: Fully automated analysis of space-based lidar data: An overview of the CALIPSO retrieval algorithms and data products. *Laser Radar Techniques for Atmospheric Sensing*, U. N. Singh, Ed., International Society for Optical Engineering (SPIE Proceedings, Vol. 5575), 16–30.
- , and Coauthors, 2009: Fully automated detection of cloud and aerosol layers in the CALIPSO lidar measurements. *J. Atmos. Oceanic Technol.*, **26**, 2034–2050.
- Warren, S. G., 1984: Optical constants of ice from the ultraviolet to the microwave. *Appl. Opt.*, **23**, 1206–1225.
- Weisz, E., J. Li, W. P. Menzel, A. K. Heidinger, B. H. Kahn, and C.-Y. Liu, 2007: Comparison of AIRS, MODIS, CloudSat and CALIPSO cloud top height retrievals. *Geophys. Res. Lett.*, **34**, L17811, doi:10.1029/2007GL030676.
- Wen, G., A. Marshak, R. F. Cahalan, L. A. Remer, and R. G. Kleidman, 2007: 3-D aerosol-cloud radiative interaction observed in collocated MODIS and ASTER images of cumulus cloud fields. *J. Geophys. Res.*, **112**, D13204, doi:10.1029/2006JD008267.
- Wielicki, B. A., R. D. Cess, M. D. King, D. A. Randall, and E. F. Harrison, 1995: Mission to planet Earth: Role of clouds and radiation in climate. *Bull. Amer. Meteor. Soc.*, **76**, 2125–2153.
- Winker, D. M., J. Pelon, and M. P. McCormick, 2003: The CALIPSO mission: Spaceborne lidar for observation of aerosols and clouds. *Lidar Remote Sensing for Industry and Environment Monitoring III*, U. N. Singh, T. Itabe, and Z. Lui, Eds., International Society for Optical Engineering (SPIE Proceedings, Vol. 4893), 1–11.
- , B. H. Hunt, and M. J. McGill, 2007: Initial performance assessment of CALIOP. *Geophys. Res. Lett.*, **34**, L19803, doi:10.1029/2007GL030135.
- , M. A. Vaughan, A. Omar, Y. Hu, K. A. Powell, Z. Liu, W. H. Hunt, and S. A. Young, 2009: Overview of the CALIPSO mission and CALIOP data processing algorithms. *J. Atmos. Oceanic Technol.*, **26**, 2310–2323.
- Wood, R., and C. S. Bretherton, 2006: On the relationship between stratiform low cloud cover and lower-tropospheric stability. *J. Climate*, **19**, 6425–6432.
- Yang, P., L. Zhang, G. Hong, S. L. Nasiri, B. A. Baum, H.-L. Huang, M. D. King, and S. Platnick, 2007: Differences between Collection 004 and 005 MODIS ice cloud optical/microphysical products and their impact on radiative forcing simulations. *IEEE Trans. Geosci. Remote Sens.*, **45**, 2886–2899.
- Yu, H., and Coauthors, 2006: A review of measurement-based assessments of the aerosol direct radiative effect and forcing. *Atmos. Chem. Phys.*, **6**, 613–666.
- Yulaeva, E., J. R. Holton, and J. M. Wallace, 1994: On the cause of the annual cycle in tropical lower-stratospheric temperatures. *J. Atmos. Sci.*, **51**, 169–174.
- Zhang, M. H., and Coauthors, 2005: Comparing clouds and their seasonal variations in 10 atmospheric general circulation models with satellite measurements. *J. Geophys. Res.*, **110**, D15S02, doi:10.1029/2004JD005021.
- Zhang, Y., W. B. Rossow, A. A. Lacis, V. Oinas, and M. I. Mishchenko, 2004: Calculation of radiative fluxes from the surface to top of atmosphere based on ISCCP and other global data sets: Refinements of the radiative transfer model and the input data. *J. Geophys. Res.*, **109**, D19105, doi:10.1029/2003JD004457.

APPENDIX: SUMMARY OF ACRONYMS AND ABBREVIATIONS.

4DVAR	Four-dimensional variational data assimilation
ADM	Atmospheric Dynamics Mission
AIRS	Atmospheric Infrared Sounder
AOD	Aerosol optical depth
APS	Aerosol polarimetry sensor
ASDC	Atmospheric Sciences Data Center
ATBD	Algorithm theoretical basis documents
BT	Brightness temperature
CALIOP	Cloud-Aerosol Lidar with Orthogonal Polarization
CALIPSO	Cloud-Aerosol Lidar and Infrared Pathfinder Satellite Observations
CCD	Charge-coupled device
CERES	Clouds and the Earth's Radiant Energy System
CNES	Centre National d'Etudes Spatiales
CNRS	Centre National de la Recherche Scientifique
CPR	Cloud profiling radar
DP	Data product
EarthCARE	Earth Clouds, Aerosols and Radiation Explorer
ECMWF	European Centre for Medium-Range Weather Forecasts
EOS	Earth Observing System
ESSP	Earth System Science Pathfinder
FOV	Field of view
GCM	General circulation model
GEOS-5	Goddard Earth Observing System, version 5
GOCART	Goddard Chemistry Aerosol Radiation Transport
HSRL	High spectral resolution lidar
ICARE	Cloud-Aerosol-Water-Radiation Interactions
IIR	Infrared Imaging Radiometer
IPSL	L'Institut Pierre-Simon Laplace
ISCCP	International Satellite Cloud Climatology Project
ITCZ	Intertropical convergence zone
LATMOS	Laboratoire Atmosphères, Milieux et Observations Spatiales
LCL	Lifting condensation level
LITE	LIDAR In-Space Technology Experiment
LMD	Laboratoire de Météorologie Dynamique
LaRC	Langley Research Center
MISR	Multangle Imaging Spectroradiometer
MODIS	Moderate Resolution Imaging Spectroradiometer
MSE	Moist static energy
NASA	National Aeronautics and Space Administration
PARASOL	Polarization and Anisotropy of Reflectances for Atmospheric Sciences Coupled with Observations from a Lidar
PROTEUS	Plate-forme Reconfigurable pour l'Observation, les Télécommunications et les Usages Scientifiques
SNR	Signal-to-noise ratio
SODERN	Société Anonyme d'Etudes et Réalisations Nucléaires
SON	September–November
TOA	Top of the atmosphere
TTL	Tropical tropopause layer
VFM	Vertical feature mask
WFC	Wide field camera